Supporting Information

Kastner et al. 10.1073/pnas.1418092112

SI Text

Second-order phase transitions often separate states that have different "symmetry properties," meaning that on one side of the transition, states remain constant when certain parameters of the system are changed, whereas states on the other side of the phase transition would be affected by the same change in parameters. Maximally informative solutions, within our model, exhibit different symmetry properties on different sides of the phase transition. Solutions in the large noise regime are not affected by an exchange in neural indexes (because the thresholds are the same for the two neurons) whereas solutions from the small noise regime are affected. In the small noise regime, the system has to arbitrarily choose a positive or a negative value by assigning one neuron to the adapting class and the other neuron to the sensitizing class. This process is directly analogous to magnetic systems where the system has to choose between two alternatives—"up" or "down" magnetization states—below the critical temperature, and thus these symmetry properties coincide with those of the Ising model. Thus, the arguments based on symmetry also indicate that the difference in thresholds, $m = \mu_2 - \mu_1$, is the neural quantity analogous to magnetization. Other quantities that have been proposed to correspond to magnetization include the mean spike rate (1) and the balance between excitation and inhibition (2). Although these quantities are potentially related to each other, and to the difference in thresholds m we describe here, in nonlinear ways, they do not produce a mapping onto one of the known types of phase transitions (1). In addition, for these other neural quantities there is not an obvious change in symmetry on different sides of the transition we identify here.

SI Methods

Experimental Preparation. We recorded from retinal ganglion cells of larval tiger salamanders, using an array of 60 electrodes (Multichannel Systems) as previously described (3). A video monitor projected the visual stimuli at 30 Hz controlled by Matlab (Mathworks), using the Psychophysics Toolbox (4, 5). Stimuli were uniform field with a constant mean intensity, M, of 10 mW/m^2 and were drawn from a Gaussian distribution. Contrast is defined as $\sigma = W/M$, where W is the SD of the intensity distribution. Neurons were probed with nine different contrast distributions from 12% to 36% in 3% intervals. The contrasts were randomly interleaved and repeated. Each contrast was presented, in total, for ≥600 s. For the calculation of the response functions, the first 10 s of data in each contrast were not used to allow for a better estimation of the steady state.

For Fig. 1 *C* and *D*, the stimulus was composed of independent 50-μm bars, each with a contrast distribution of 35%. The fact that the stimulus was spatial made the effective contrast experienced by the cell unknown. However, the contrast for the normalization was estimated by comparing the values of the slopes to those recorded with a spatially uniform stimulus (Fig. 2*B*).

Modeling Neural Responses Using Linear–Nonlinear Models. LN models consisted of the light intensity passed through a linear temporal filter, which describes the average response to a brief flash of light, followed by a static nonlinearity, which describes the threshold and sensitivity of the cell. To compute the model, the stimulus, $s(t)$, was convolved with a linear temporal filter, $F(t)$, which was computed as the time reverse of the spike-triggered average stimulus, such that $g(t) = \int F(t-\tau)s(\tau)d\tau$. A static nonlinearity, $N(g)$, was computed by comparing all values of the firing rate, $r(t)$, with $g(t)$, and then computing the average value of $r(t)$ over bins of $g(t)$. The filter, $F(t)$, was normalized in amplitude such that it did not amplify the stimulus; i.e., the variances of s and g were equal (6). Thus, the linear filter contained only relative temporal sensitivity, and the nonlinearity represented the overall sensitivity of the transformation. The nonlinearity was fitted using a logistic function

$$P(\text{spike}\,|\,x) = \left[1 + \exp\left[\frac{-(x-\mu)}{\nu}\right]\right]^{-1} \qquad \textbf{[S1]}$$

that has two parameters: threshold μ corresponding to a 50% spiking probability and the slope ν of the function (Fig. 1*A*). This functional form is advantageous because it matches well the input functions of single neurons (7), and it represents a minimal function consistent with the constraints on the mean firing rate and mean filtered stimulus, x, given a spike (8).

Information Maximization. The mutual information between the filtered stimulus values and the neural responses becomes a function of four parameters: a threshold and a slope value for each of the two neurons. The response functions for each neuron from Eq. **S1** together define the probability of observing one of the four possible responses of the two neurons given a filtered stimulus x. The four response patterns r_i correspond to the presence or absence of a spike from each of the two neurons. This treats the neurons as conditionally independent without significant correlations in their responses for a given input, which is a good first approximation for the fast Off adapting and sensitizing cells (3).

The mutual information is equal to the difference between the so-called total entropy and the noise entropy (9). The noise entropy represents the uncertainty in neural responses induced by the input noise. For conditionally independent responses, the noise entropy is the sum of uncertainties of individual neurons considered separately. The uncertainty in neural responses is small for inputs that are either much less or much greater than μ, because for such inputs, the spike probability remains close to 0 or 1, respectively. However, for input values close to the threshold μ, the probability to elicit a spike is close to 0.5, which indicates maximal uncertainty in the neural response to repeated presentations of such inputs. This uncertainty can be quantified as the entropy of the neural response for a given stimulus x:

$$S_i(x) = -\sum p(r_i\,|\,x)\log_2 p(r_i\,|\,x). \qquad \textbf{[S2]}$$

As shown in Fig. S1*D* this quantity reaches the peak value of 1 for $x = \mu$ and decreases to zero with increasing $|x-\mu|$. The larger the slope ν is, the larger the range of input values with the spike probability close to 0.5. The noise entropy, $H(r|x)$, is computed by averaging this quantity across inputs x and the two neurons:

$$H(r\,|\,x) = -\int p(x)\sum_{i=1}^{2}\sum_{p_i=0}^{1} p(r_i\,|\,x)\log_2 p(r_i\,|\,x)dx. \qquad \textbf{[S3]}$$

As shown in Fig. S1*E*, the noise entropy increases with ν.

From the response functions $p(r_i|x)$ one can also compute the average probability of observing r_i by multiplying the response functions by the input distribution and averaging with respect to $p(x)$. The total entropy, $H(r)$, is computed as an entropy

representing the four possible response patterns r_i reflecting the presence or absence of a spike from each of the two neurons:

$$H(r) = -\sum p(r_i)\log_2 p(r_i). \quad \textbf{[S4]}$$

Metabolic Constraints on Information Maximization. Achievable information transmission rates generally increase with metabolic resources (7, 10–12). However, this does not diminish the potential relevance of solutions with lower information rates if they have lower metabolic requirements. Therefore, we seek to find maximally informative solutions among parameter values that have comparable metabolic requirements. In the context of our model, the variables that could serve as proxies for the metabolic cost are the average spike rate across the two retinal ganglion cells (13, 14) and noise in the afferent circuitry, with smaller ν implying a higher metabolic cost. The average spike rate is primarily determined by the average threshold $\bar{\mu} = (\mu_1 + \mu_2)/2$. Therefore, we consider information for a given pair of values ν_1 and ν_2 as a function of $\mu_1 - \mu_2$ while adjusting $\bar{\mu}$ to ensure that all solutions correspond to the same average spike rate. As shown in Fig. 3 and Fig. S4, changing the value of the spike rate constraint (and therefore $\bar{\mu}$) leads only to quantitative changes in the information function and does not alter qualitatively the dependence on the other parameters. An example of optimal threshold separation is shown in Fig. S1*F*. When extracting the parameters for the threshold μ and slope ν from measured response functions, the data were normalized by their maximal firing rate to ensure that they ranged from 0 to 1.

Spinodal Line and Model Normalization. The spinodal line in Fig. 3 was extracted from the curves that related the information to the threshold difference between the two response functions (Fig. 2*C*) and is defined as the point between the minimum and maximum of the information where the derivative of information with respect to the threshold difference, m, is maximal. The spinodal points were determined for each pair of fast Off adapting and sensitizing cells at each contrast.

1. Yu S, Yang H, Shriki O, Plenz D (2013) Universal organization of resting brain activity at the thermodynamic critical point. *Front Syst Neurosci* 7:42.
2. Shew WL, Yang H, Yu S, Roy R, Plenz D (2011) Information capacity and transmission are maximized in balanced cortical networks with neuronal avalanches. *J Neurosci* 31(1):55–63.
3. Kastner DB, Baccus SA (2011) Coordinated dynamic encoding in the retina using opposing forms of plasticity. *Nat Neurosci* 14(10):1317–1322.
4. Brainard DH (1997) The Psychophysics toolbox. *Spat Vis* 10(4):433–436.
5. Pelli DG (1997) The VideoToolbox software for visual psychophysics: Transforming numbers into movies. *Spat Vis* 10(4):437–442.
6. Baccus SA, Meister M (2002) Fast and slow contrast adaptation in retinal circuitry. *Neuron* 36(5):909–919.
7. Pitkow X, Meister M (2012) Decorrelation and efficient coding by retinal ganglion cells. *Nat Neurosci* 15(4):628–635.
8. Fitzgerald JD, Sincich LC, Sharpee TO (2011) Minimal models of multidimensional computations. *PLoS Comput Biol* 7(3):e1001111.
9. Brenner N, Strong SP, Koberle R, Bialek W, de Ruyter van Steveninck RR (2000) Synergy in a neural code. *Neural Comput* 12(7):1531–1552.
10. Doi E, et al. (2012) Efficient coding of spatial information in the primate retina. *J Neurosci* 32(46):16256–16264.
11. Borghuis BG, Ratliff CP, Smith RG, Sterling P, Balasubramanian V (2008) Design of a neuronal array. *J Neurosci* 28(12):3178–3189.
12. Ratliff CP, Borghuis BG, Kao YH, Sterling P, Balasubramanian V (2010) Retina is structured to process an excess of darkness in natural scenes. *Proc Natl Acad Sci USA* 107(40):17368–17373.
13. Balasubramanian V, Berry MJ, 2nd (2002) A test of metabolically efficient coding in the retina. *Network* 13(4):531–552.
14. Laughlin SB, de Ruyter van Steveninck RR, Anderson JC (1998) The metabolic cost of neural information. *Nat Neurosci* 1(1):36–41.

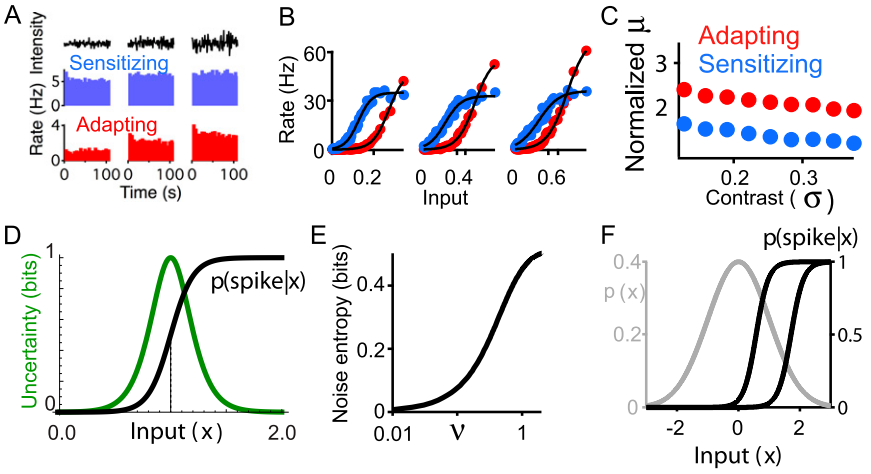

Fig. S1. Experimental paradigm and model setup. (*A*) Example neural responses for different levels of contrast. Stimulus (*Top*) and average response of a fast Off sensitizing (*Middle*) and adapting (*Bottom*) cell are recorded simultaneously. (*B*) Steady-state nonlinearities for the same pair of adapting and sensitizing cells recorded simultaneously at three different levels of temporal contrast: 12% (*Left*), 24% (*Center*), and 36% (*Right*). Black lines are the sigmoid fits to the data. (*C*) Adapting cells maintain higher thresholds than sensitizing cells across a range of contrasts. Symbols show average midpoint of the sigmoid, μ, normalized by contrast, σ, for all sensitizing ($n = 11$) and adapting ($n = 36$) cells at each contrast. Error values, SEM, are smaller than symbols. (*D*) Uncertainty in the neural response peaks near the threshold value. The uncertainty was evaluated according to Eq. **S2**. (*E*) The noise entropy, evaluated according to Eq. **S3**, increases with increasing slope, ν, for a single response function and a fixed value of $\langle r \rangle$. (*F*) An example of the maximally informative placement of two response functions for a given input distribution (gray line) and average response rate $\langle r \rangle$ shows the separation of thresholds between the two cell types.

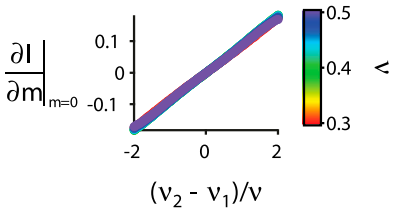

Fig. S2. The difference in slopes of neural response functions is analogous to a magnetic (conjugate) field. In physics, a magnetic field induces a linear change in the average magnetization regardless of temperature. More specifically, in the Ising model, the value of the magnetic field can be found by taking the derivative of free energy with respect to magnetization at one of the optima. Performing an analogous procedure in the neural context amounts to evaluating the derivative of information with respect to m, for $m = 0$. This yields a function that is proportional to the difference of the slopes of the two response functions $\nu_2 - \nu_1$, confirming that the latter quantity can be used as a proxy for the magnetic field. The analysis was repeated for multiple values of ν in different colors. The lines overlay, thereby obscuring the different colors.

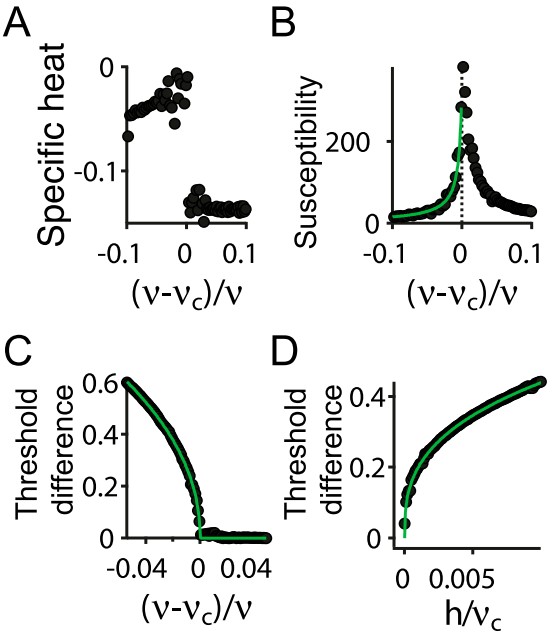

Fig. S3. Singular behavior of maximally informative solutions near the critical point matches the Ising model. (*A*) The analog of the specific heat, the second derivative of the information, I, with respect to the noise, $C = \partial^2 I/\partial\nu^2$, exhibits a drop expected from mean-field calculations for the Ising model for $\nu > \nu_c$ (1). (*B*) The analog of the magnetic susceptibility, the second derivative $\chi = \partial^2 I/\partial h^2$ of the information, I, with respect to $h = \nu_2 - \nu_1$, the quantity analogous to a magnetic field, diverges as $|\nu - \nu_c|^{-1}$. The fit (green line) yields an exponent of −0.93, which matches the value of −1 predicted by the mean-field theory for the magnetic susceptibility. (*C*) The optimal threshold difference between response functions as a function of the slope, ν, follows the theoretically predicted equation $m \propto \sqrt{|\nu - \nu_c|}$ dependence, when $h = 0$. The fit of the relationship yields $m \propto |\nu - \nu_c|^{0.47}$ (green line). (*D*) Optimal threshold difference as a function of the slope difference, h, a quantity analogous to a magnetic field, for $\nu = \nu_c$ follows the predicted dependence of $m \propto h^{1/3}$. The fit of the relationship yields $m \propto h^{0.34}$ (green line). The functions in *A*–*C* are plotted relative to $(\nu - \nu_c)/\nu$, the normalized distance to the critical point, such that zero indicates that ν is at the critical noise value. This difference is normalized by ν according to the definition from ref. 2 to obtain a dimensionless quantity, analogous to reduced temperature. All exponents take similar values whether the reduced effective temperature is defined as $|\nu - \nu_c|/\nu$ according to ref. 2 or as $|\nu - \nu_c|/\nu_c$.

1. Landau LD, Lifshitz EM (1978) *Statistical Physics* (Pergamon, Oxford).
2. Kardar M (2007) *Statistical Physics of Fields* (Cambridge Univ Press, New York).

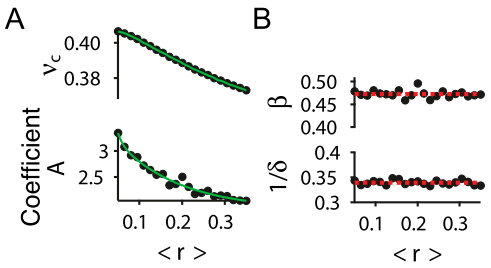

Fig. S4. Changes in model parameters with changes in the rate constraint. (*A*) Model parameters other than the universal scaling exponents, β and $1/\delta$, vary smoothly with $\langle r \rangle$. (*Top*) the relationship between the critical noise value ν_c and $\langle r \rangle$. (*Bottom*) The relationship between the proportionality coefficient *A*, from the fit to the model for the equation $m = A|\nu - \nu_c|^{\beta}$ when $h = 0$ (Fig. S3*C*), and different $\langle r \rangle$. (*B*) The scaling exponents β (*Top*) and $1/\delta$ (*Bottom*) do not vary with the average rate, $\langle r \rangle$. Dotted red lines show the average values for the two exponents (0.47 and 0.34, respectively).

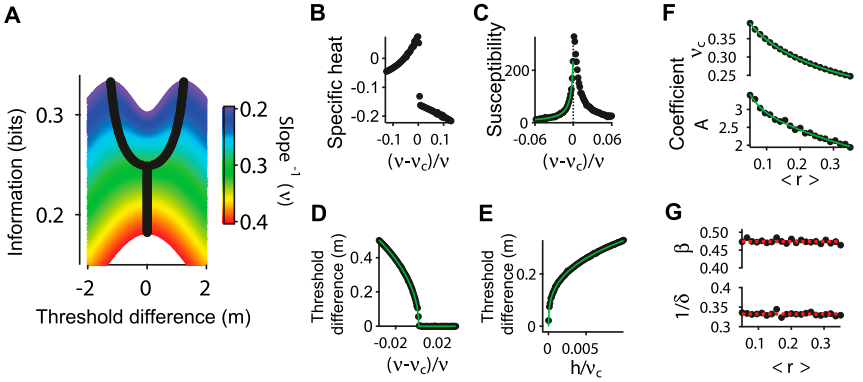

Fig. S5. Analysis of the critical point for non-Gaussian inputs. The quantitative characteristics of the critical point are preserved when non-Gaussian inputs $P(x) \propto e^{-|x|}$ were used instead of a Gaussian distribution. (*A*) analogous to Fig. 1*B*; (*B–E*) analogous to Fig. S3; (*F* and *G*) analogous to Fig. S4.

Table S1. Summary of predictions for critical exponents for the nearest-neighbor Ising model in different dimensions

Exponent	2D Ising	3D Ising	4D Ising/mean field	Experiments in various physical systems	Our measurements in the retina
β	1/8 = 0.125	0.325 ± 0.0015	1/2 = 0.5	0.316–0.35	0.39 ± 0.12
δ	15	4.82(4)	3	4.2–4.9	7 ± 4

Data represent compilation of table 3.1 from ref. 1 and table 3.4 from ref. 2 in comparison with our measurements. The values for the four-dimensional model coincide with values obtained using mean-field theory and with values assuming an infinite range of interactions (2).

1. Goldenfeld N (1992) *Lectures on Phase Transitions and the Renormalization Group* (Addison-Wesley, Reading, MA).
2. Stanley HE (1971) *Introduction to Phase Transitions and Critical Phenomena* (Oxford Univ Press, New York).